AIAA 2002-1512

# Structural Response of Compression-Loaded, Tow-Placed, Variable Stiffness Panels

K. Chauncey Wu
NASA Langley Research Center
Hampton, Virginia

Zafer Gürdal
Virginia Polytechnic Institute and State University
Blacksburg, Virginia

James H. Starnes, Jr.
NASA Langley Research Center
Hampton, Virginia

43rd AIAA/ASME/ASCE/AHS/ASC
Structures, Structural Dynamics and Materials Conference
22-25 April 2002
Denver, Colorado

AIAA 2002-1512

# STRUCTURAL RESPONSE OF COMPRESSION-LOADED, TOW-PLACED, VARIABLE STIFFNESS COMPOSITE PANELS

K. Chauncey Wu*
NASA Langley Research Center
Hampton, Virginia 23681

Zafer Gürdal†
Virginia Polytechnic Institute and State University
Blacksburg, Virginia 24061

James H. Starnes, Jr.§
NASA Langley Research Center
Hampton, Virginia 23681

## Abstract

Results of an analytical and experimental study to characterize the structural response of two compression-loaded variable stiffness composite panels are presented and discussed. These variable stiffness panels are advanced composite structures, in which tows are laid down along precise curvilinear paths within each ply and the fiber orientation angle varies continuously throughout each ply. The panels are manufactured from AS4/977-3 graphite-epoxy pre-preg material using an advanced tow placement system. Both variable stiffness panels have the same layup, but one panel has overlapping tow bands and the other panel has a constant-thickness laminate. A baseline cross-ply panel is also analyzed and tested for comparative purposes. Tests performed on the variable stiffness panels show a linear prebuckling load-deflection response, followed by a nonlinear response to failure at loads between 4 and 53 percent greater than the baseline panel failure load. The structural response of the variable stiffness panels is also evaluated using finite element analyses. Nonlinear analyses of the variable stiffness panels are performed which include mechanical and thermal prestresses. Results from analyses that include thermal prestress conditions correlate well with measured variable stiffness panel results. The predicted response of the baseline panel also correlates well with measured results.

## Introduction

The increasing use of polymer composite materials in aerospace vehicles has stimulated the development of sophisticated manufacturing technology for their fabrication. One significant advancement in machine tool technology is the introduction of commercial systems for precise, repeatable placement of pre-preg composite tows. One such advanced tow placement system is the Viper¶ Fiber Placement System[1] (FPS) from Cincinnati Machine. These advanced tow placement systems enable fabrication of advanced composite structures, where the fibers in any given ply may be laid down along curvilinear paths.

In an advanced composite structure, the fiber orientation angle is therefore allowed to vary con-

* Aerospace Engineer, Vehicle Analysis Branch.
† Professor, Departments of Aerospace and Ocean Engineering, and Engineering Science and Mechanics, Associate Fellow AIAA.
§ Senior Engineer, Structures and Materials Competency, Fellow AIAA.



¶ Identification of commercial products and companies in this paper is used to describe the materials adequately. The identification of these commercial products does not constitute endorsement, expressed or implied, of such products by the National Aeronautics and Space Administration.

tinuously within each ply and throughout the structure, and is not required to be straight and parallel in each ply as in conventional composite structures. Because their stiffness properties also vary continuously over the domain of the structure, these configurations are referred to herein as "variable stiffness" structures. A convention for the definition of tow paths for rectangular variable stiffness panels is first introduced in Ref. 2. A reference tow path is defined which passes through the center of the panel, and has a linear variation of the fiber orientation angle over a specified distance in one direction, referred to as the variation axis. Additional tow paths are then generated within a ply by indexing the reference tow path by fixed increments along the so-called shift axis, which is orthogonal to the variation axis.

Analytical studies[2,3] indicate that significant increases in buckling load are possible for square, simply-supported variable stiffness panels that are subjected to in-plane loads when compared to equal-weight, conventional angle-ply laminates. These optimized designs tend to have fiber orientation angles that are more orthogonal to the load axis near the panel centerline, and more parallel to the load axis near the panel edges. Thus, the center of the panel has a low stiffness in the loading direction, with a greater percentage of the load supported by the stiffer edge regions of the panel.

The response of variable stiffness panels subject to a manufacturing constraint on fiber radius-of-curvature is evaluated in Ref. 4. The in-plane response of symmetric variable stiffness laminates with regions of overlapping tow bands (generated by placement of adjacent tows during the manufacturing process) is evaluated in Ref. 5. These overlapping tow bands form local areas of increased thickness in the laminate that resemble discrete stiffeners on the panel surface, and are more complicated to model than the constant-thickness laminates studied previously. An overview of the selection of a variable stiffness panel design for fabrication, as well as some details on the fabrication of two first-generation variable stiffness panels, is presented in Ref. 6.

Unique issues arising from the fabrication of the variable stiffness panels in Ref. 6 are presented and discussed in more detail in Ref. 7, along with results of an experimental study to determine the coefficients of thermal expansion of the variable stiffness panels when subjected to thermal loads. Comparisons are also made to results from classical lamination theory. The present paper is a follow-on study to Ref. 7, and presents the results of an experimental program to characterize and evaluate the structural response of variable stiffness panels subjected to compression loads by mechanical end shortening. These results are compared to the response of a conventional cross-ply panel fabricated using the same materials and processes. In addition, results of analytical studies to predict the structural response of the variable stiffness panels are also presented and compared to test results.

## Test Specimens and Test Apparatus

This section contains an overview of the panels evaluated in this study, the procedures used to prepare the panels for testing, and the equipment used to test the panels and record their response.

### Variable stiffness panels

A variable stiffness panel design with a nominal $[\pm 45/(90\pm\langle 30|60\rangle)_4]_S$ 20-ply layup has been chosen for fabrication. Following the convention used in Refs. 3 and 4, the (90+<30|60>) notation designates one variable stiffness ply with a +30 deg. fiber orientation angle at the panel center and a +60 deg. fiber orientation angle at ±12 in. along the variation axis, which is then rotated by 90 deg. until it is parallel to the global Y-axis (see Fig. 1). The reference tow path for this variable stiffness ply is shown as a bold line in Fig. 1. Also shown in the figure are the additional tow paths generated by shifting the reference tow path through fixed increments along the shift axis (parallel to the X-axis load direction). Straight-fiber ±45 deg. plies are also placed on the front and back surfaces of the panel, surrounding the 16 variable stiffness plies.

Three 26-in.-long by 24.5-in.-wide composite panels have been fabricated using AS4/977-3 graphite-epoxy pre-preg material. The Viper FPS used to fabricate these panels has the capacity to place up to 24, 1/8-in.-wide pre-preg tows during each pass of the tow placement head. Two panels have the variable stiffness layup described previously, but one panel has overlapping tow bands and the other panel does not. For the first variable stiffness panel, hereafter designated as the panel with overlaps, all 24 pre-preg tows are applied during each pass of the tow placement head, causing overlaps between tows from adjacent

passes to occur towards the panel edges. Because the variable stiffness panels are laid up on a flat tool surface, the resulting thickness distribution is asymmetric, with a raised stiffener pattern on only one side of this panel. The second variable stiffness panel, designated as the panel without overlaps, uses the tow-cut/restart capability of the Viper FPS to maintain a nominal 20-ply thickness across the panel while applying the variable stiffness layup. Use of this tow-cut/restart capability may result in resin-rich pockets or voids within the panel. The third panel, designated as the baseline panel, has a conventional $[\pm 45]_{5s}$ layup and is used to provide a reference for comparing the performance of the two variable stiffness panels.

**Support fixtures**

The variable stiffness panels are prepared for testing by mounting the panels in specially-designed support fixtures. These support fixtures are designed to mechanically straighten the panel edges before the tests are performed, and are necessary because of the large anticlastic imperfections, attributed to the fabrication scheme,[7] which are present in the cured variable stiffness panels. Since the baseline panel has a conventional straight-fiber laminate, with much smaller imperfections than the variable stiffness panels, simplified versions of these fixtures that have a minimal capability to straighten the panel edges are used for the baseline panel.

The support fixtures attached to the variable stiffness panel perimeter are also designed to enforce test boundary conditions along the panel edges, and approximate simply-supported (on the vertical edges in the test configuration) and clamped (on the horizontal edges) boundary conditions. The clamped-end support fixtures also serve as molds to contain an epoxy potting compound used to prevent brooming failure on the loaded edges of the panel. These boundary conditions ensure that the variable stiffness panels will respond more like a flat panel when loaded in compression. The panel with overlaps is shown in Fig. 2 after the panel edges have been straightened using the support fixtures.

**Geometric imperfections**

The geometric shapes of the three composite panels have been measured with a coordinate measuring machine before the support fixtures were installed to establish their as-manufactured, unloaded, reference shapes.[7] After the support fixtures have been attached, the back surfaces of the three panels were again surveyed to determine the geometric imperfections. The coordinate measuring machine can locate a point in space with an accuracy of ±0.0003 in. within its workspace. Out-of-plane measurements were taken at a grid of points within the 24-in.-square test sections. The machined loading surfaces of all three panels were also surveyed and found to be flat within 0.0005 in. root-mean-square (RMS), and parallel to within 0.5 degree.

After the back surface of the panel with overlaps was surveyed, panel thickness data from a previous survey[7] are used to infer the coordinates of the panel's front surface. The projected front surface imperfections of the panel with overlaps are shown in Fig. 3 after installation of the fixtures. The maximum imperfection amplitude for this panel is 0.033 in. and the minimum amplitude is -0.040 in., with a 0.016-in. RMS amplitude. This process is then repeated for the panel without overlaps, where the maximum imperfection amplitude is measured as 0.042 in., the minimum amplitude is -0.030 in., with a 0.016-in. RMS amplitude.

When compared to the imperfection amplitudes for the variable stiffness panels without support fixtures reported in Ref. 7, installation of the fixtures reduces the imperfection amplitudes in these panels by an order of magnitude. Without fixtures, the maximum imperfection amplitude for the panel with overlaps is 0.331 in., the minimum amplitude is -0.383 in., and the RMS amplitude is 0.152 in. Similar reductions are also observed for the panel without overlaps.

However, use of the fixtures to flatten the variable stiffness panels also induces some unknown stress state into the panels prior to testing. This stress state is associated with deformation of the variable stiffness panels by the support fixtures, since the panels would be extremely difficult to test with mechanical loads with their large as-manufactured imperfections. Necessary care must also be taken during the analyses of the variable stiffness panels to account for the stresses induced by attachment of these support fixtures. To this end, a mechanical prestress case, associated with installation of the support fixtures, will be defined as an applied displacement field

between the measured configurations with and without support fixtures.

The baseline panel has also been surveyed after its support fixtures were installed. With the fixtures, this panel has a maximum amplitude of 0.033 in., a minimum amplitude of -0.076 in., and an RMS amplitude of 0.025 in. These new imperfections are actually greater than the results reported for this panel in Ref. 7. Some of the differences between these two sets of measurements may be due to distortions of the baseline panel induced during attachment of the fixtures. Additional variations may result from surveying the back surfaces of the panels, which have a rough, slightly pebbled finish. The measurements in Ref. 7 are taken on the front surfaces of the panels, which are formed on a smooth tool surface during manufacture, resulting in smaller variations than measurements taken on the back surfaces.

**Test apparatus**

The three composite panels have been loaded by axial compression loads with quasi-static applied displacements at load rates of between 1.5 and 2 kips/minute in a 300-kip capacity electromechanical test stand. The axial force applied to the panels during the mechanical end shortening tests is measured with a load cell permanently mounted to the test stand. Surface strains are measured at discrete locations on the panels during the tests using electrical-resistance strain gages. Axial displacement data are measured using linear variable displacement transducers (LVDTs) located at the four corners of the test stand platens, while deflections normal to the panel are measured with a LVDT located at the panel center. All electronic data are recorded using a mainframe-based data acquisition system. Qualitative full-field normal displacement measurements are obtained using shadow moiré interferometry, and recorded with both still and video cameras.

Axial and transverse strains on the front and back surfaces of the panel are measured using between 26 and 34 strain gages that are bonded to the panel surfaces using procedures described in Ref. 8. The nominal strain gage patterns used for the three panels are illustrated in Ref. 7. All of the strain gages are installed as back-to-back gage pairs. Various combinations of axial and transverse gage pairs are positioned on the axial and transverse centerlines of the variable stiffness and baseline panels. In addition to the gages shown in Ref. 7, four pairs of back-to-back axial gages are installed across the transverse centerline of the baseline panel.

## Analysis Method and Analysis Models

Structural analyses of the variable stiffness and baseline panels have been performed using the finite element analysis method. The STAGS nonlinear shell analysis code[9] has been used to perform buckling and nonlinear analyses of the panels to predict their structural response. In this section, the analysis models used to predict the panel response are presented and discussed. The measured geometric imperfections discussed previously are included in the variable stiffness and baseline panel analysis models.

**Finite element model**

The finite element model used for the analyses of the variable stiffness panels is shown in Fig. 4. This model has 3021 nodes and a 26-in.-long by 24.5-in.-wide rectangular planform. The majority of the 2912 elements in the models are 0.5-in.-square, although some elements are as small as 0.25-in.-square. The finite element used for these analyses is the STAGS 410-type general shell element with both membrane and bending stiffnesses. As discussed in Ref. 7, mechanical properties for an AS4/977-3 ply, determined from laminate-level coupon tests, are $E_1$=18.83 Msi, $E_2$=1.34 Msi, $G_{12}$=0.74 Msi and $\nu_{12}$=0.36. The measured ply coefficients of thermal expansion are $\alpha_1$ = –0.19 μin./in./deg. F and $\alpha_2$ = 19.1 μin./in./deg. F. The average ply thickness for the panel with overlaps and baseline panel is 0.00765 in., and is 0.00745 in. for the panel without overlaps. An analysis model with mostly 1-in.-square elements (not shown) has been developed for analyses of the baseline panel. The baseline panel model does not require the same level of refinement as the variable stiffness panel models because it does not have the ply angle or laminate thickness variations that are present in the variable stiffness panels.

**Boundary conditions**

The nominal boundary conditions selected for the analysis models are designed to replicate the test boundary conditions described previously. These constraints approximate the test boundary

conditions applied with the potting compound and support fixtures, as well as the loads applied to the panel during the tests. The vertical edge support fixtures are modeled with w=0 displacements and $R_Y$=0 rotations applied on the left and right vertical edges of the panel model. These simple support boundary conditions are shown as long-dashed lines in Fig. 4.

The potting compound and end fixture restraints on motion of the panel ends are modeled with w=0 displacements along the short-dashed lines in the shaded areas of Fig. 4. In-plane displacements are set to v=0 on the vertical edges within the potting compound (the end points of the short-dashed lines) to model the potting compound's restraint on the panel's Poisson expansion. These boundary conditions therefore assume that the potting compound has an infinite stiffness. Fully-clamped boundary conditions are applied to the panel bottom edge, and partially-clamped boundary conditions with a uniform end shortening (where u=constant, and all other degrees-of-freedom are set equal to zero) are applied along the panel top edge.

**Variable stiffness laminate modeling**

Special purpose software has been written to determine the number of plies and fiber orientation angles in the variable stiffness laminate at a grid of discrete points across the panel planform. The input for these codes is the manufacturing data for the variable stiffness panels provided by Cincinnati Machine. These files contain information regarding the number of tows placed and tow placement head coordinates during each pass made by the Viper FPS.

The analysis model laminate thicknesses for the panel with overlaps are shown in Fig. 5. This figure shows the highly discretized nature of the model, with many discontinuities in element thicknesses. The modeled laminate thickness varies between 0.291 and 0.153 in., or 38 and 20 plies. These thickness variations cause local eccentricities in the laminate. Because the variable stiffness panel is laid up on a flat tool surface, all of the thickness variations occur only on one side of the laminate, resulting in the possible introduction of local bending loads.

The computed fiber orientation angles in one ply of the finite element model of the panel without overlaps are shown in Fig. 6. The fiber orientation angles range from approximately –30 deg. near the simply supported panel edges to almost –60 deg. on the panel centerline, and are constant within each ply of each element. As noted previously, the tow-cut/restart capability of the Viper FPS is used during manufacture of this panel to eliminate the thickness variations present in the panel with overlaps. However, use of this capability also results in finite gaps between tow bands within each ply of the panel without overlaps, which are not modeled in this representation of the structure.

## Results and Discussion

Results of mechanical end shortening tests performed on the baseline panel and two variable stiffness panels are presented in this section. Selected shadow moiré photographs, strain and displacement data are presented and discussed. Geometrically nonlinear analyses and bifurcation buckling computations are performed for the three panels. Linear prebuckling stiffnesses, bifurcation buckling and transition loads are computed. The effect of thermal and mechanical prestress conditions on variable stiffness panel response are also quantified and discussed. Qualitative and quantitative comparisons are made between measured and predicted deflections and strains.

**Baseline panel**

**Test results**

Results from a mechanical load test of the baseline panel subjected to axial compression loads are presented in this section. The maximum mechanical load applied during this test is 8 kips, which is well into the postbuckling load range for this panel. The measured axial load for this panel is plotted in Fig. 7 as a function of the average axial end shortening from the four LVDTs located at the platen corners. The curve shown in this figure displays a significant degree of nonlinearity in transitioning from an initial linear prebuckling response to a highly nonlinear postbuckling response. The nonlinearity in the baseline panel response is due in part to the presence of geometric imperfections in the test specimen, and makes unambiguous identification of a buckling load difficult. For example, the transition from lin-

ear to nonlinear behavior in the figure starting around 3.5 kips suggests that panel buckling occurs somewhere in excess of this load level.

Therefore, for the tests and nonlinear analyses presented in the present paper, a transition load is defined as the load where the linear prebuckling axial response intersects the nonlinear portion of the panel response. For computational purposes, the transition load is equal to the load level where the ratio of the secant stiffness (load divided by end shortening) to the linear prebuckling stiffness is equal to 0.995. For the baseline panel test data shown in the plot, the prebuckling stiffness $K_o$ (computed as the least-squares best-fit slope between 1.5 and 3.5 kips) is 512.5 kips/in. and the transition load $P_{tr}$ is 3.8 kips, as listed in Table 1. The end shortening corresponding to this transition load is 0.007 in., or 0.03 percent axial strain after dividing by the nominal 26-in. panel length.

The measured axial load is plotted in Fig. 8 as a function of the panel center normal deflection, which reaches a value of 0.153 in. (the average baseline panel thickness) at 5.6 kips. The deflections shown in the figure increase with increasing load, with the panel center moving along the +Z-axis in Fig. 4. The influence of the geometric imperfections is also readily apparent, as the deflection increases rapidly from its theoretical prebuckling value of zero (for a perfectly flat panel). The baseline panel is observed to buckle in a mode shape that has a half-sine wave in both the axial and transverse directions.

The measured axial loads are plotted as functions of the axial and transverse strains at the panel center in Fig. 9. The panel front and back strains diverge gradually at loads below about 4 kips, then much more rapidly as the load increases. The axial bending strain (the difference between the front and back strains for gages of the same orientation) increases until it is equal to the axial membrane strain (the average of the front and back strains) at 4.8 kips. The axial bending strain then increases until it is almost twice the axial membrane strain at the 8-kip maximum load. For the transverse gages, the bending strain increases until it is nearly equal in magnitude to the membrane strain at 8 kips.

The baseline panel was subsequently loaded to failure, which occurred at the failure load $P_{fail}$ of 26.9 kips listed in Table 1. The corresponding end shortening at failure of 0.334 in. is equal to an axial strain of 1.28 percent. Examination of the panel after conclusion of the test shows that failure originates at the middle of one edge of the panel in the simple support boundary condition, then propagates towards the center of the panel. The middle of this panel edge pulled completely out of the simple support fixture, but it is not known if this happened before or after the panel failed. If this edge pulled out of the support fixture before the panel failed, it could cause the panel to fail at a much lower load than if the edge were fully supported throughout the test.

**Analysis results and correlation**

An eigenvalue analysis has been performed to compute the bifurcation buckling loads and prebuckling stiffnesses of the baseline composite panel using the model and boundary conditions described previously. As listed in Table 2a, the predicted prebuckling stiffness $K_o$ (computed as the inverse of the end shortening generated by a unit axial load) for the baseline panel is 513.7 kips/in. and the buckling load $P_{cr}$ is 5.3 kips. The predicted mode shape from this analysis is the same as that observed during the baseline panel test.

A geometrically nonlinear analysis was then performed to predict the baseline panel response to an applied end shortening. As for the test data, the prebuckling stiffness is computed as the slope of the least-squares best-fit to the linear portion of the panel response. The prebuckling stiffness $K_o$ of 505.5 kips/in. (shown in Table 2b) from the nonlinear analysis is 1.4 percent less than the measured panel stiffness, and the predicted transition load $P_{tr}$ of 3.6 kips is 5.3 percent less than the measured transition load.

The predicted load for the baseline panel is then plotted as a function of the end shortening in Fig. 7, and panel center normal deflections in Fig. 8, along with the corresponding test data. The measured and predicted curves compare very well for loads up to 8 kips and, except for minor differences, are virtually identical. The axial loads are plotted as functions of the analytical and measured panel center strains in Fig. 9. The measured and predicted data also correlate well, with some differences observed between the back surface strain curves. The correlation observed between the test data and analytical results indi-

cates that the nonlinear analyses with measured imperfections are an excellent prediction of the baseline panel response.

**Panel with overlaps**

**Test results**

Test results for the panel with overlaps are presented and discussed in this section. The measured axial load is shown in Fig. 10 as a function of the average end shortening. For the test data presented in the figure, the prebuckling stiffness $K_o$ (computed as the least-squares best-fit slope between 2 and 13 kips) of the panel with overlaps is 649.9 kips/in. and the transition load $P_{tr}$ is 13.6 kips, as listed in Table 1. The measured prebuckling stiffness of the panel with overlaps is 27 percent greater than the baseline panel value, and the transition load of the panel with overlaps is almost 3.6 times the baseline panel transition load. The end shortening corresponding to the measured transition load is 0.021 in., or 0.08 percent axial strain.

The measured axial load is plotted as a function of the panel center normal deflection in Fig. 11. The 18.2-kip load level where the deflection is equal to the 0.184-in. average wall thickness is also indicative of the nonlinear behavior of this panel. The maximum deflection at the panel center is 0.917 in., which approaches the 1-in. stroke limit of the LVDT. A shadow moiré photograph of the out-of-plane deflections at 16 kips load is shown in Fig. 12. The panel mode shape exhibits a half-sine wave in both the axial and transverse directions. The maximum deflection at 16 kips is only about 0.1 in., as shown by the small number of fringes, and does not occur at the panel center (indicated with a circle in the figure), but to the right of center on the transverse centerline.

The axial load is plotted as a function of the measured axial and transverse strains at the panel center in Fig. 13. Divergence of the front and back strain gage pairs occurs gradually beginning at approximately 10 kips, and very rapidly after about 15 kips load. The axial membrane strain increases in a bilinear fashion with increasing axial load. At the maximum load, the bending strain computed from the axial strains is almost as large as the axial membrane strain. The transverse membrane strain increases almost linearly up to panel failure.

As listed in Table 1, the panel failure load $P_{fail}$ is 41.1 kips, or 3 times the transition load. The end shortening at failure is 0.130 in., an axial strain of 0.50 percent and over 6 times the transition strain. Noises were heard during the test at loads between 28 and 40.7 kips, and several discontinuities are evident in the deflection and strain data at loads corresponding to the noises heard during the test. A shadow moiré photograph of the normal deflections at 40 kips load is shown in Fig. 14. The mode shape is the same as that observed in Fig. 12, although the deflection amplitude is much greater as evidenced by the larger number of fringes in the figure. As noted previously, the maximum normal deflection occurs on the transverse centerline approximately 2.5 in. to the right of the panel center.

**Structural analyses**

Buckling and nonlinear analyses have been performed for the panel with overlaps and measured geometric imperfections, and the results of these analyses are presented in this section. Linear prebuckling stiffnesses, buckling and transition loads have been computed from the results of these analyses. Two different prestress conditions, mechanical prestresses corresponding to the panel edge straightening, and thermal prestresses from the difference between operational and curing temperatures, are modeled in the nonlinear analyses. Comparisons are also made between measured and predicted deflections and strains.

An eigenvalue analysis has been performed to compute the buckling load and prebuckling stiffness of the panel with overlaps, with results listed in Table 2a. No prestress conditions are included for this analysis, as indicated in the table. The predicted prebuckling stiffness $K_o$ for this panel is 694.5 kips/in., and the predicted buckling load $P_{cr}$ is 11.6 kips. The panel mode shape from these analyses has a half-sine wave in both the axial and transverse directions.

Next, a nonlinear analysis without prestresses has been performed for the panel with overlaps. Although the deflection and strain data from this analysis are not presented, the transition load and prebuckling stiffness have been computed and are shown in Table 2b. The predicted prebuckling stiffness $K_o$ is 684.5 kips/in., which is 5.3 percent greater than the test value. The computed transition load $P_{tr}$ is 9.0 kips, or 34 percent less than

the measured result. Considering the complexity of the panel with overlaps and the simplifications required to model the panel, good agreement is observed for the prebuckling stiffness. However, the significant difference evident between the analytical and experimental transition loads indicates that the preliminary analysis without prestresses is not a good predictor of the behavior of this variable stiffness panel.

**Prestress conditions**

Some additional factor (or factors) is responsible for the differences between the measured and predicted behavior of the variable stiffness panels. One possibility is that the panel edge straightening, performed to reduce the anticlastic shape from the manufacturing process, induces a tensile prestress state in the panel, thus leading to a higher buckling load. Analytical studies[10] also indicate that inclusion of thermal curing stresses can have a beneficial effect on the buckling load of plates and shells. Both of these prestress conditions are now examined and evaluated using finite element analyses.

The analysis model and procedures for the panel with overlaps have been modified to include the effect of an induced stress state generated by the mechanical edge straightening process. As described previously, the unstressed, unfixtured variable stiffness panel has a severe anticlastic shape. A geometrically nonlinear analysis has been performed to apply out-of-plane displacements that force the panel model from the measured anticlastic configuration of Ref. 7 into the measured configuration with support fixtures shown in Fig. 3. Boundary conditions are applied at the corners to prevent panel rigid-body motion during this analysis. The internal stress state and panel geometry resulting from this analysis are then used as input for a subsequent nonlinear analysis with an applied end shortening load and test boundary conditions shown in Fig. 4.

Another possible cause of the differences observed in the analytical and measured panel with overlaps responses are the residual thermal curing stresses. A thermal prestress condition is generated within the variable stiffness laminate by cooling the panel from the 350 deg. F cure temperature to the 70 deg. F test temperature. An analysis procedure has been developed to evaluate the effect of the thermal prestresses on the response of the panel with overlaps. A –280 deg. F thermal load was applied in a linear analysis of the panel, with the panel out-of-plane geometry constrained to the fixtured configuration shown in Fig. 3. The in-plane displacements of the panel ends within the potting compound were then constrained to values generated from the thermal analysis, and a nonlinear analysis with an applied end shortening and test boundary conditions was performed. A –280 deg. F thermal load was also maintained during the nonlinear analysis.

**Analysis results and correlation**

A nonlinear analysis with mechanical prestresses has been performed for the panel with overlaps, and the resulting axial load is plotted as a function of the end shortening in Fig. 10. The analytical prebuckling stiffness $K_o$ of 688.7 kips/in., listed in Table 2b, is 6 percent greater than the measured panel stiffness. The predicted transition load $P_{tr}$ of 14.2 kips is 4.4 percent greater than the measured transition load. The transition load from the analysis with mechanical prestresses is significantly greater than the value predicted in the preliminary analysis, and much closer to the measured value. For any given load level, the measured end shortening is greater than the analytical response, with larger differences observed in the postbuckling load region up to panel failure.

The predicted end shortening from a nonlinear analysis including thermal prestresses is also plotted in Fig. 10. The prebuckling stiffness $K_o$ of 687.6 kips/in. from this analysis is 5.8 percent greater than the experimental panel stiffness. However, the computed transition load $P_{tr}$ of 12.8 kips for the nonlinear analysis with thermal prestresses is 6 percent less than the corresponding value from the test. A qualitative evaluation of the end shortening results shown in the figure suggests that both of the analyses with prestresses correlate well with the measured behavior of the panel with overlaps up to about 20 kips.

Computed panel center normal deflections from the analyses with prestresses are plotted with the test data in Fig. 11. The deflections shown in the figure all increase along the +Z-axis in Fig. 4 with increasing axial load. The measured deflection matches the predicted response from the analysis with thermal prestresses up to about 10 kips, then parallels the response from the analysis with mechanical prestresses to approxi-

mately 20 kips. The test data are bounded by the two analytical curves between 12 and 28 kips. Predicted out-of-plane displacements at an applied end shortening of 0.130 in. from an analysis with thermal prestresses are shown as a contour plot in Fig. 15. The predicted maximum deflection of 0.907 in. is slightly below the panel center (indicated with a circle) in the figure. These displacement contours are qualitatively very similar to the out-of-plane deformations observed with shadow moiré interferometry during the test. However, the experimental results indicate that the actual maximum deflection occurs on the transverse centerline.

The measured and predicted axial and transverse strains at the panel center are compared in Fig. 13. The measured axial strains closely match the predicted axial strains from the analysis with mechanical prestresses up to loads of about 28 kips and, to a lesser degree, the axial strains from the analysis with thermal prestresses. The measured transverse strains, while smaller in magnitude than the axial strains, show very good agreement with the strains from the analysis with mechanical prestresses. Good qualitative correlation is observed between the test results and the transverse strains predicted by the analysis with thermal prestresses. A qualitative evaluation of the results presented for the panel with overlaps suggests that, while results from the analysis with thermal prestresses compare well with measured data, the correlation between the test data and the results from the analysis with mechanical prestresses is much better.

## Panel without overlaps

### Test results

Test results for the panel without overlaps are presented in this section. The measured axial compressive load is plotted as a function of the average axial end shortening in Fig. 16. The prebuckling stiffness $K_o$ for this panel, equal to the least-squares best-fit slope between 2 and 9 kips, is 534.8 kips/in. and the transition load $P_{tr}$ is computed as 9.2 kips. Both values are listed in Table 1. The prebuckling stiffness of the panel without overlaps is 4.4 percent greater than the baseline panel stiffness, and much less than the 27 percent stiffness increase observed for the panel with overlaps. The transition load of the panel without overlaps is almost 2.5 times the baseline panel transition load, a significant improvement in performance over the baseline panel. The measured end shortening corresponding to the transition load is 0.017 in., or 0.07 percent axial strain. The panel without overlaps also has a more pronounced bilinear axial response than that of the panel with overlaps.

The axial load is plotted as a function of the panel center normal deflection in Fig. 17 for the panel without overlaps. For loads below about 9 kips, the deflection is relatively small, and is equal to the 0.149-in. average wall thickness at 10.8 kips load. The maximum deflection at the panel center exceeds the 1-in. linear limit of the LVDT at 27.4 kips load. The shadow moiré photographs taken during this test show that this panel has the same mode shape as observed for the panel with overlaps, although the displacement contours are more oval for this panel.

The axial loads are plotted as functions of the measured panel center axial and transverse strains in Fig. 18 for the panel without overlaps. For loads below 8 kips, divergence of the front and back strains occurs much more gradually than for the panel with overlaps. The strains diverge rapidly above 10 kips, which suggests that panel buckling occurs somewhere in this load range. The axial strain data show the same behavior observed for the panel with overlaps, where the bending strain increases to become as large as the membrane strain as the load increases. However, the bending strain component for the transverse gages remains relatively small up to failure.

Failure of the panel without overlaps occurs at a failure load $P_{fail}$ of 28.1 kips, as indicated in Table 1. The average end shortening at failure is 0.163 in., or an axial strain of 0.63 percent. The failure load is 3.1 times greater than the transition load, which is close to the ratio computed for the panel with overlaps. However, the failure strain for this panel is 9.6 times the transition strain, or 1.5 times the ratio for the panel with overlaps.

### Structural analyses

The buckling and nonlinear analyses described previously have also been performed for the panel without overlaps. Results from these analyses, including prebuckling stiffnesses, buckling and transition loads, are presented in this section. Results from nonlinear analyses performed with the two prestress conditions de-

scribed previously are also compared to measured data.

An eigenvalue analysis has been performed to compute the buckling load for the panel without overlaps, with the results listed in Table 2a. Measured geometric imperfections are included for the analyses of this panel. The computed prebuckling stiffness $K_o$ of 557.4 kips/in. is 25 percent less than the corresponding stiffness of the panel with overlaps, and the predicted buckling load $P_{cr}$ of 6.0 kips is about half of the computed buckling load for the panel with overlaps. The predicted mode shape from these analyses is the same as described previously.

A nonlinear analysis without prestresses was also performed for the panel without overlaps. Results from this analysis (see Table 2b) show that the computed prebuckling stiffness $K_o$ of 556.3 kips/in. is 4 percent greater than the measured stiffness. However, the predicted transition load $P_{tr}$ of 6.0 kips is about 35 percent less than the experimental transition load for the panel without overlaps. This observation confirms that the analysis without prestresses is insufficient to model correctly the response of this variable stiffness panel.

**Analysis results and correlation**

The mechanical edge straightening and the –280 deg. F thermal prestress cases discussed previously are also applied to the panel without overlaps to evaluate their effect on the predicted response, and the results are discussed in this section. The end shortening predicted from an analysis with mechanical prestresses is shown in Fig. 16. The analytical prebuckling stiffness $K_o$ of 543.3 kips/in. in Table 2b is only 1.6 percent greater than the measured panel stiffness. The predicted transition load $P_{tr}$ from this analysis is 7.0 kips, which is 24 percent less than the corresponding test value. As for the panel with overlaps, the end shortening curves correlate well at lower loads (up to about 20 kips here), then diverge at an increasing rate. The predicted end shortening at the failure load level for the panel without overlaps is much less than the measured end shortening.

The predicted load for the analysis with thermal prestresses is also plotted as a function of the end shortening in Fig. 16. The prebuckling stiffness $K_o$ of 553.5 kips/in. predicted from this analysis is 3.5 percent greater than the measured value, and the transition load $P_{tr}$ of 8.5 kips is within 8 percent of the measured transition load. The measured and predicted postbuckling response curves match well to approximately 15 kips, which shows that both analyses with prestresses are good predictors of the axial response of the panel without overlaps at lower load levels.

The panel center normal deflections from the analyses with prestresses are plotted in Fig. 17 with the experimental results. The data are plotted here as absolute values because the predicted deflection from the analysis with mechanical prestresses is in the opposite direction of the deflections from both the analysis with thermal prestresses and, more importantly, the test, which both increase along the +Z-axis with increasing load. The measured deflection closely matches the predicted response from the analysis with thermal prestresses up to 8 kips, then parallels the response out to approximately 0.2 in. deflection. In both analysis cases, the predicted panel mode shape has a half-sine wave in the axial and transverse directions.

Predicted panel center axial and transverse strains from the analyses of the panel without overlaps are plotted in Fig. 18, along with measured strain data. The measured strain data show very good agreement with predictions from the analysis with thermal prestresses. This correlation begins to degenerate at an applied load of about 15 kips for the axial strains, but continues up to panel failure for the transverse strains. Because the panel center deflects in the opposite direction for the analysis with mechanical prestresses, the strains from this analysis do not correlate well with results from the analysis with thermal prestresses or from the test.

Since the results from the analysis with thermal prestresses correlate well with the test data, they are considered a much better prediction of the behavior of the panel without overlaps than the analysis with mechanical prestresses. Because similar analyses were performed for both variable stiffness panels, the results presented in this section suggest that the nonlinear analyses with thermal prestresses provide more consistently accurate predictions for the behavior of the variable stiffness panels.

**Discussion**

The relative performance gains achieved using the variable stiffness panels are presented and discussed in this section. Measured performance data for the baseline panel are used as normalizing factors for comparison of the variable stiffness panel results. The panel prebuckling stiffness values from Table 1 are divided by the nominal 26-in. panel length to determine EA, the panel extensional stiffness. These results are reported in Table 3 in both raw form and normalized by the baseline panel extensional stiffness. A 4 percent improvement in normalized extensional stiffness is observed for the panel without overlaps, and a more significant increase of 27 percent for the panel with overlaps.

The measured extensional stiffnesses, transition loads and failure loads are then divided by the measured weights of the three composite panels[7] to evaluate the panel's performance on an equal-weight basis. Results are again presented in raw and normalized forms in Table 3. When the increased weight of the panel with overlaps (20 percent greater than the baseline panel weight) is taken into account, its normalized extensional stiffness-to-weight ratio is about equal to that of the panel without overlaps, with an average 7 percent improvement over the corresponding value for the baseline panel.

The transition load-to-weight comparison in Table 3 shows that the panel with overlaps has a normalized transition load that is 3 times greater than the baseline panel, and a 20 percent increase over the panel without overlaps. The weight-normalized failure load for the panel without overlaps is 8 percent greater than the baseline panel, and 28 percent greater than the baseline panel for the panel with overlaps. Thus, significant increases in structural efficiency are achievable using the variable stiffness concept.

## Concluding Remarks

Advanced tow placement systems for precise, repeatable placement of composite pre-preg tows are an enabling technology for the fabrication of advanced, variable stiffness composite structures, where the fiber orientation angle varies continuously within each ply and throughout the structure. Two variable stiffness panels, one with overlapping tow bands and one without overlapping tow bands, and a baseline cross-ply panel have been fabricated using an advanced tow placement system. The structural responses of the three panels subjected to compression loads are compared.

The results of mechanical end shortening tests of the variable stiffness and baseline panels are presented and discussed in the present paper. Both variable stiffness panels have significantly better structural efficiency than the baseline panel. The panel with overlaps also has a much higher efficiency than the panel without overlaps. Measured results for the variable stiffness panels exceed initial analytical predictions, which suggest that the buckling load for the panel without overlaps should be about 40 percent greater than the buckling load of the baseline panel.

Experimental data show that the panel without overlaps has a transition load (where the linear prebuckling axial response intersects the nonlinear portion of the panel response) of almost 2.5 times the baseline panel transition load. In addition, the transition load for the panel with overlaps is about 3.6 times the baseline panel transition load. Failure loads of the variable stiffness panels are between one and 1.5 times the baseline panel failure load. Some portion of these efficiency increases is due to the use of a variable stiffness layup. The differences in structural response observed for the two variable stiffness panels are most likely due to the overlapping tow bands on the panel with overlaps, which serve as local stiffeners to increase that panel's load-carrying capability.

Because the measured improvements are much greater than predicted by the preliminary analyses, nonlinear finite element analyses with prestresses have been performed to correlate better the predictions with test results. Two prestress cases, a mechanical edge straightening performed to prepare the variable stiffness panels for test, and a –280 deg. F thermal load to simulate the residual stresses associated with the panel curing process, are modeled in this study. Results from both analyses with mechanical and thermal prestresses correlate well with the test data for the panel with overlaps. However, only results from the analysis with thermal prestresses show good correlation with test results for the panel without overlaps. The analyses with thermal prestresses show a more consistent correlation with test results than the analyses with mechanical prestresses for the variable stiffness panels.

Therefore, the analyses with thermal prestresses are considered to provide a better prediction of the behavior of the variable stiffness panels.

Some of the differences observed between test and analysis results for the panel with overlaps may be due to the highly discretized nature of its analysis model, which has discontinuous laminate thicknesses and fiber orientation angles across the elements. The finite element model of the panel without overlaps also has discontinuous fiber orientation angles, but with a uniform laminate thickness in each element. Analytical predictions of the baseline panel response correlate well with experimental data.

The nonlinear finite element analysis techniques used in this study appear to generate acceptable results for the variable stiffness and baseline panels. Additional mesh refinement may yield better correlation between test and analysis results. Mesh refinement of the variable stiffness panel models would also result in a corresponding refinement of the fiber orientation angles for both panels, as well as refinement of the laminate thickness distribution for the panel with overlaps.

## References


1. Evans, D. O., Vaniglia, M. M., and Hopkins, P. C., "Fiber Placement Process Study," 34th *International SAMPE Symposium*, Vol. 34, Book 2, May 1989, pp. 1822-1833.

2. Gürdal, Z., and Olmedo, R., "In-Plane Response of Laminates with Spatially Varying Fiber Orientations: Variable Stiffness Concept," *AIAA Journal*, Vol. 31, No. 4, April 1993, pp. 751-758.

3. Olmedo, R., and Gürdal, Z., "Buckling Response of Laminates with Spatially Varying Fiber Orientations," *Proceedings of 34th AIAA/ASME/ASCE/AHS/ASC Structures, Structural Dynamics, and Materials Conference*, April 19-21, 1993, La Jolla, CA, pp. 2261-2269. Available as AIAA 93-1567.

4. Waldhart, C., Gürdal, Z., and Ribbens, C., "Analysis of Tow-Placed, Parallel Fiber, Variable Stiffness Laminates," *Proceedings of 37th AIAA/ASME/ASCE/AHS/ASC Structures, Structural Dynamics, and Materials Conference*, April 15-17, 1996, Salt Lake City, UT. Available as AIAA 96-1569.

5. Langley, P. T., "Finite Element Modeling of Tow-Placed Variable-Stiffness Composite Laminates," M. S. Thesis, Virginia Polytechnic Institute and State University, 1999.

6. Tatting B. F., and Gürdal, Z., "Design and Manufacture of Tow-Placed Variable Stiffness Composite Laminates with Manufacturing Considerations," *Proceedings of 13th U.S. National Congress of Applied Mechanics*, June 21-26, 1998, Gainesville, FL.

7. Wu, K. C. and Gürdal, Z., "Thermal Testing of Tow-Placed, Variable Stiffness Panels," *Proceedings of the 42nd AIAA/ASME/ASCE/AHS/ASC Structures, Structural Dynamics and Materials Conference*, Seattle, Washington, April 16-19, 2001. Available as AIAA 2001-1190.

8. Moore, T. C., Sr., "Recommended Strain Gage Application Procedures for Various Langley Research Center Balances and Test Articles," NASA TM-110327, March 1997.

9. Rankin, C. C., et al., *STAGS User Manual, version 4.0*, Lockheed Martin Missiles & Space Co., Inc., Palo Alto, CA. June 2000.

10. Foldager, J. P., Hansen, J. S., and Olhoff, N., "Optimization of the Buckling Load for Composite Structures Taking Thermal Effects into Account," *Structural and Multidisciplinary Optimization*, Vol. 21, Springer-Verlag, 2001, pp. 14-31.

Table 1: Measured performance of baseline and variable stiffness panels

| Panel | $K_o$, kips/in. | $P_{tr}$, kips | $P_{fail}$, kips |
|---|---|---|---|
| Baseline panel | 512.5 | 3.8 | 26.9 |
| Panel with overlaps | 649.9 | 13.6 | 41.1 |
| Panel without overlaps | 534.8 | 9.2 | 28.1 |

Table 2: Predicted performance for baseline and variable stiffness panels

a: Eigenvalue analysis

| Baseline panel panel | | Prestress case | Panel with overlaps | | Panel without overlaps | |
|---|---|---|---|---|---|---|
| $K_o$, kips/in. | $P_{cr}$, kips | | $K_o$, kips/in. | $P_{cr}$, kips | $K_o$, kips/in. | $P_{cr}$, kips |
| 513.7 | 5.3 | None | 694.5 | 11.6 | 557.4 | 6.0 |

b: Nonlinear analysis

| Baseline panel panel | | Prestress case | Panel with overlaps | | Panel without overlaps | |
|---|---|---|---|---|---|---|
| $K_o$, kips/in. | $P_{tr}$, kips | | $K_o$, kips/in. | $P_{tr}$, kips | $K_o$, kips/in. | $P_{tr}$, kips |
| 505.5 | 3.6 | None | 684.5 | 9.0 | 556.3 | 6.0 |
| | | Mech. | 688.7 | 14.2 | 543.3 | 7.0 |
| | | Therm. | 687.6 | 12.8 | 553.5 | 8.5 |

Table 3: Performance comparison for baseline and variable stiffness panels

| Panel | EA, x $10^6$ lb | Weight, lb | EA/wt., x $10^6$ | $P_{tr}$/wt., x $10^3$ | $P_{fail}$/wt., x $10^3$ |
|---|---|---|---|---|---|
| Baseline panel | 13.33 (1)* | 5.65 | 2.36 (1) | 0.67 (1) | 4.76 (1) |
| Panel with overlaps | 16.90 (1.27) | 6.77 | 2.50 (1.06) | 2.01 (2.99) | 6.07 (1.28) |
| Panel without overlaps | 13.90 (1.04) | 5.48 | 2.54 (1.08) | 1.68 (2.50) | 5.13 (1.08) |

* Quantities normalized by baseline panel values are shown in parentheses

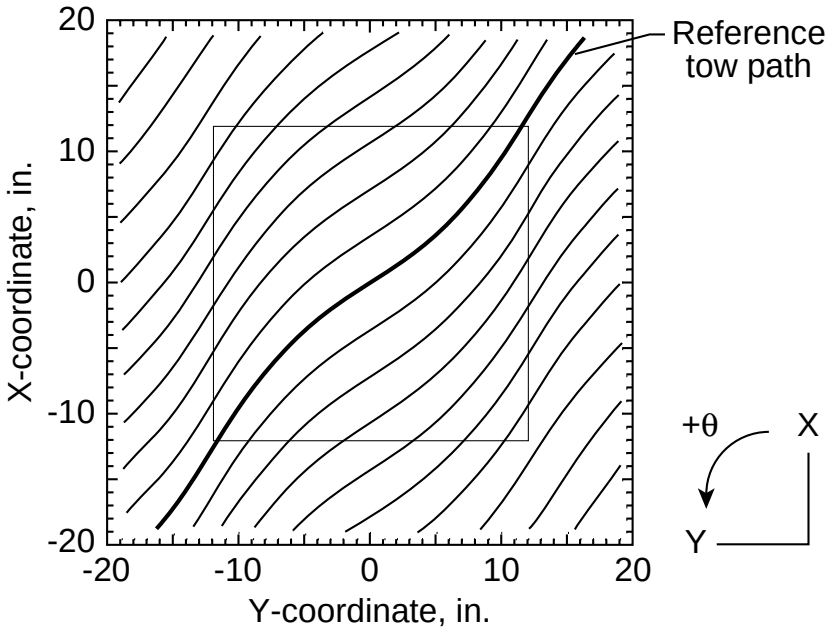


1. Tow placement head centerline paths for variable stiffness ply.

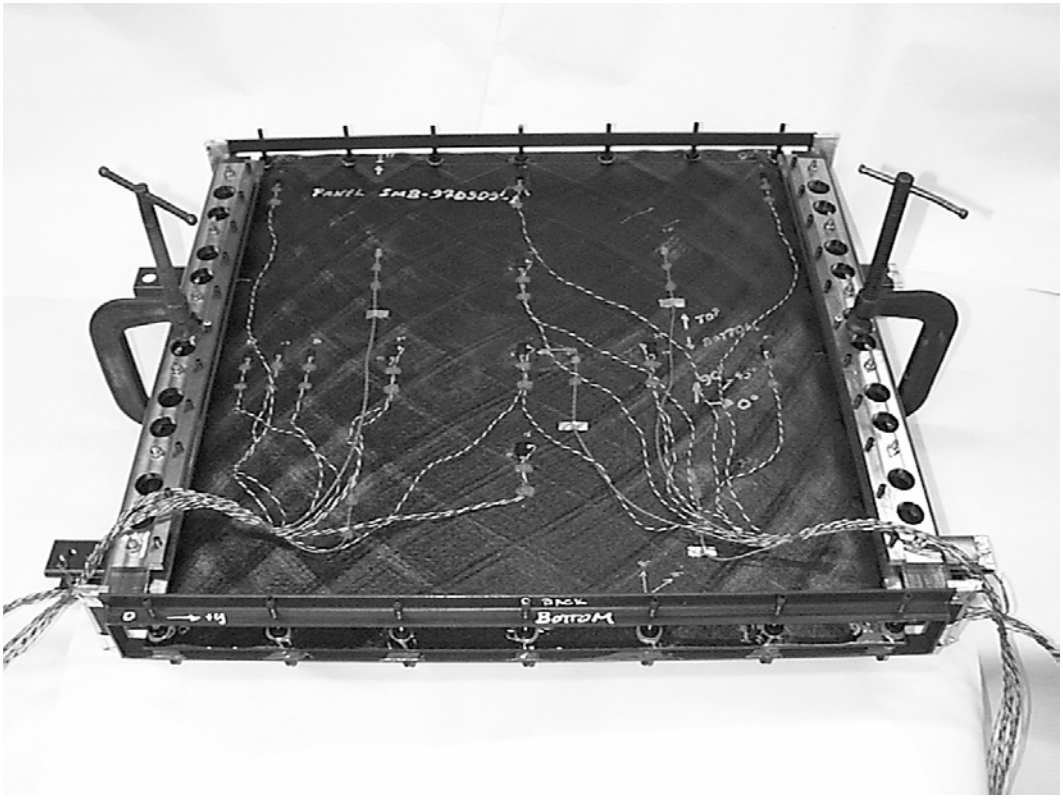

2. Support fixtures installed on panel with overlaps.


3. Measured imperfections for panel with overlaps.

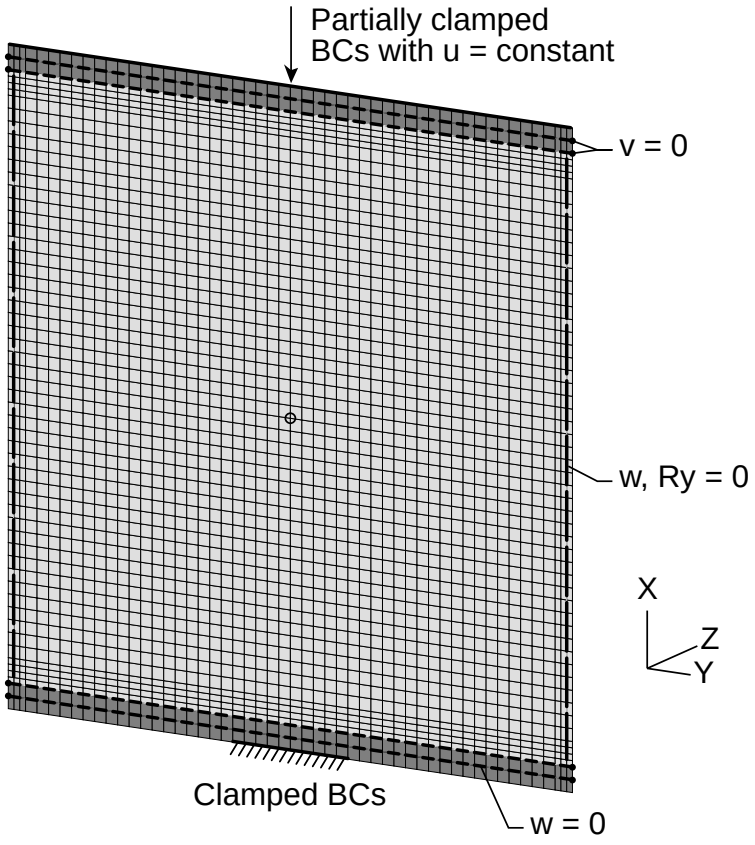


4. Finite element model of variable stiffness panel.

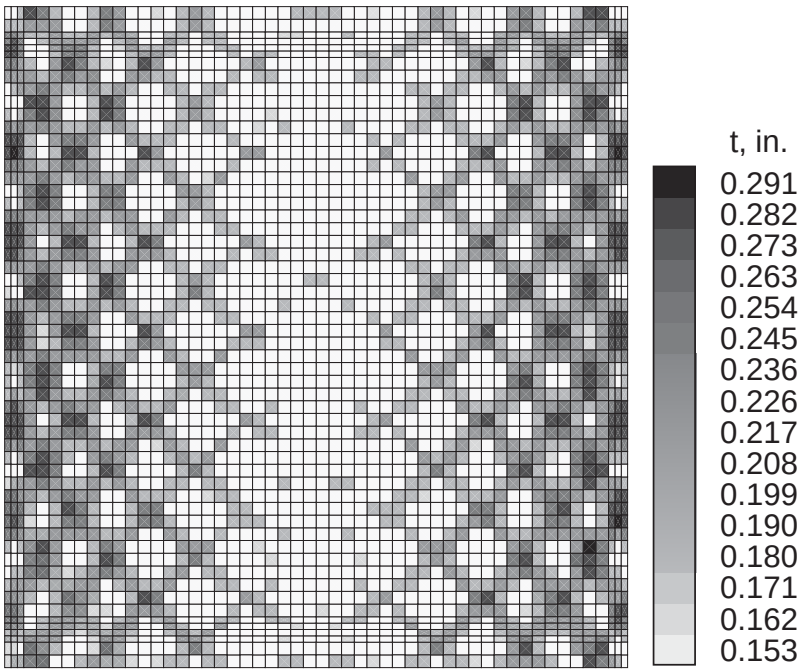


5. Laminate thicknesses for panel with overlaps.

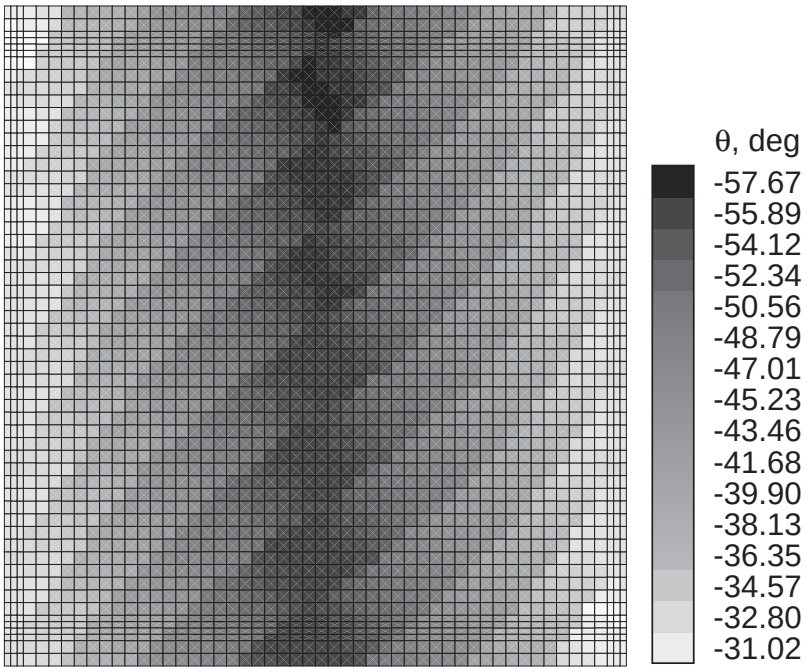


6. Fiber orientation angles for panel without overlaps.

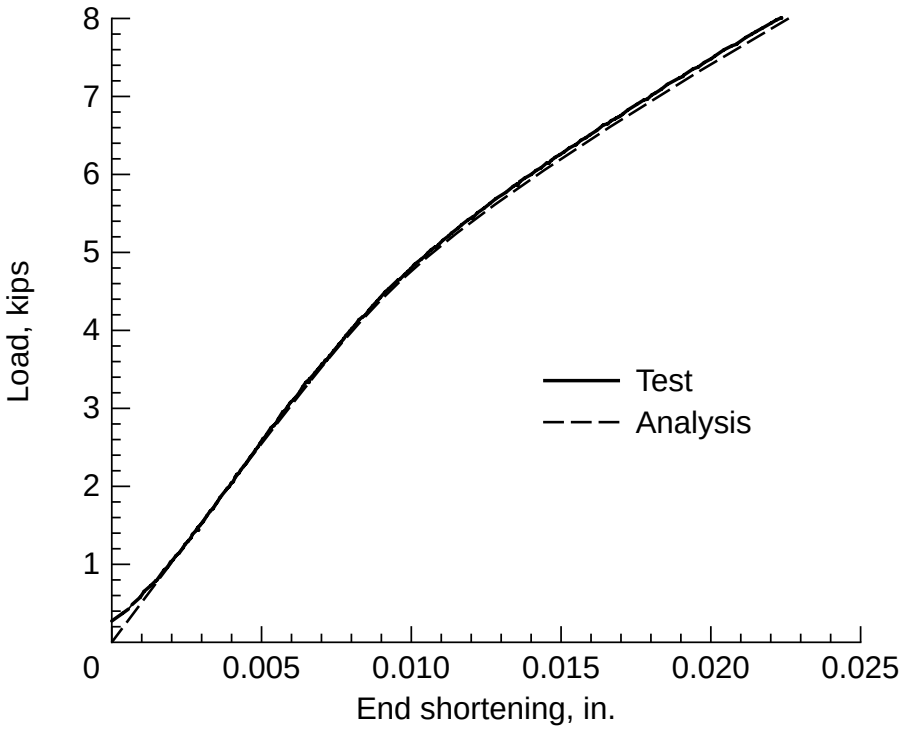


7. End shortening curves for baseline panel.

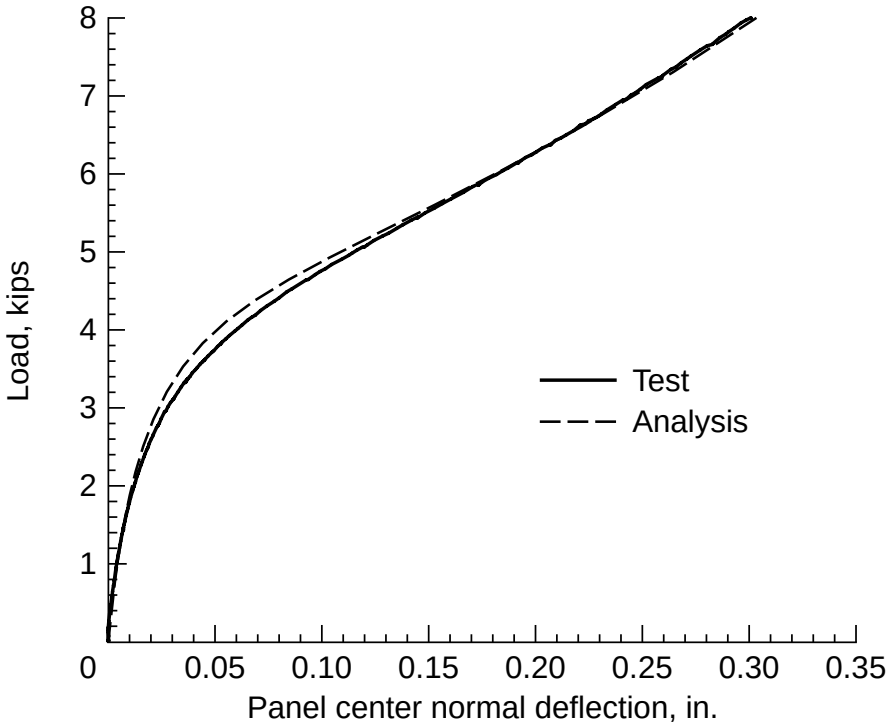


8. Panel center normal deflection curves for baseline panel.

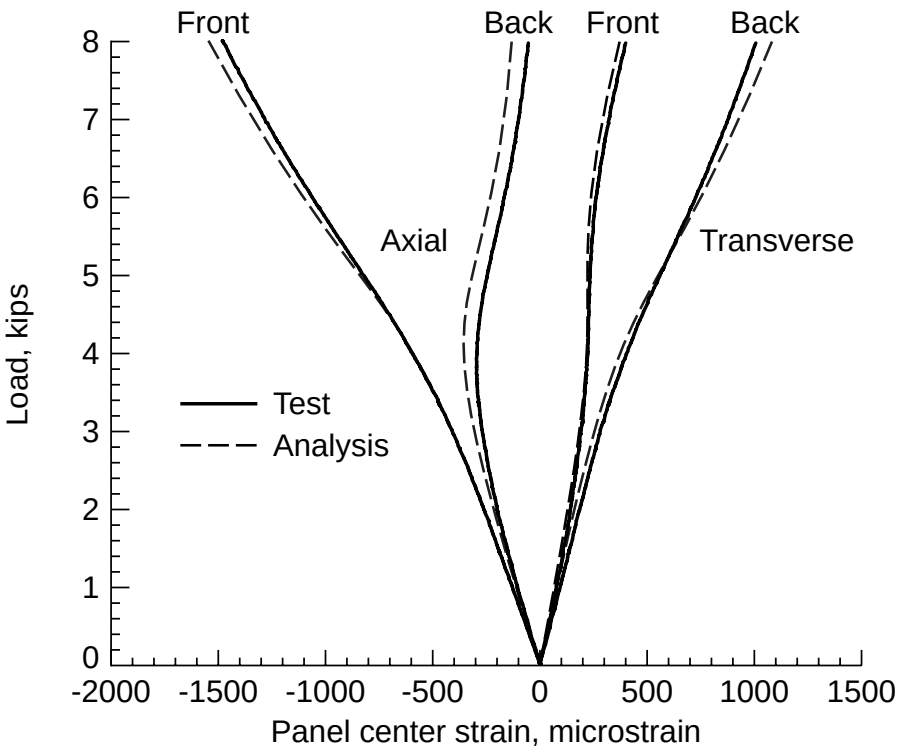


9. Panel center strain curves for baseline panel.

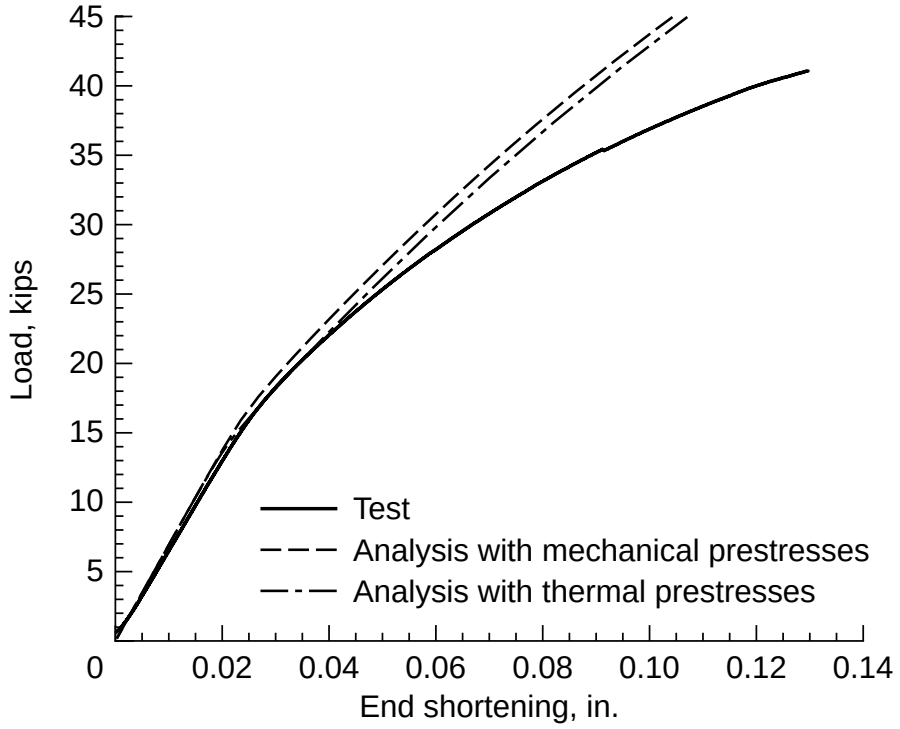


10. End shortening curves for panel with overlaps.

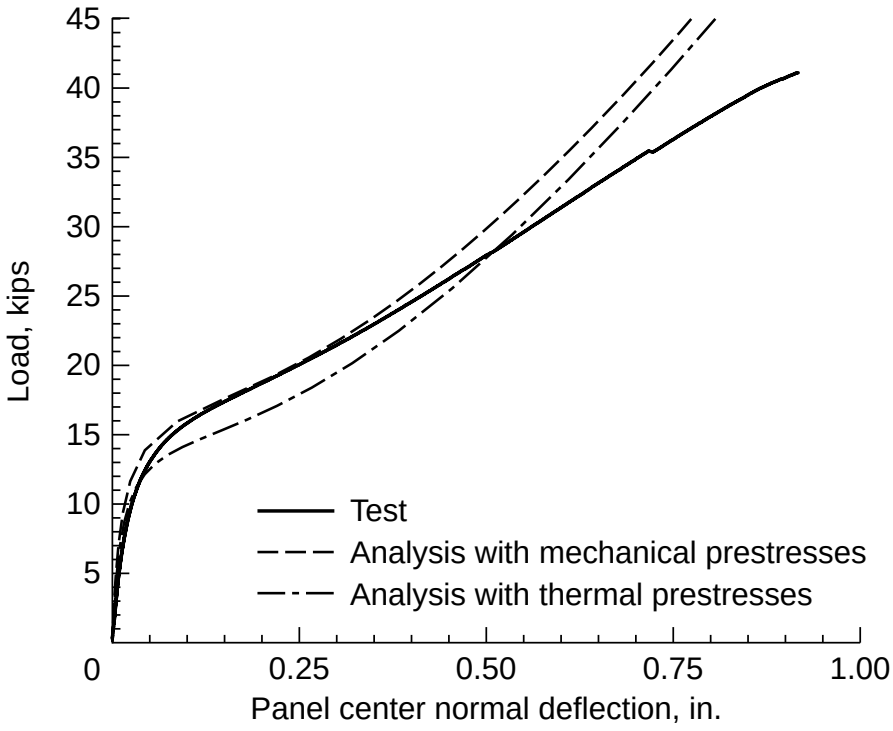


11. Panel center normal deflection curves for panel with overlaps.

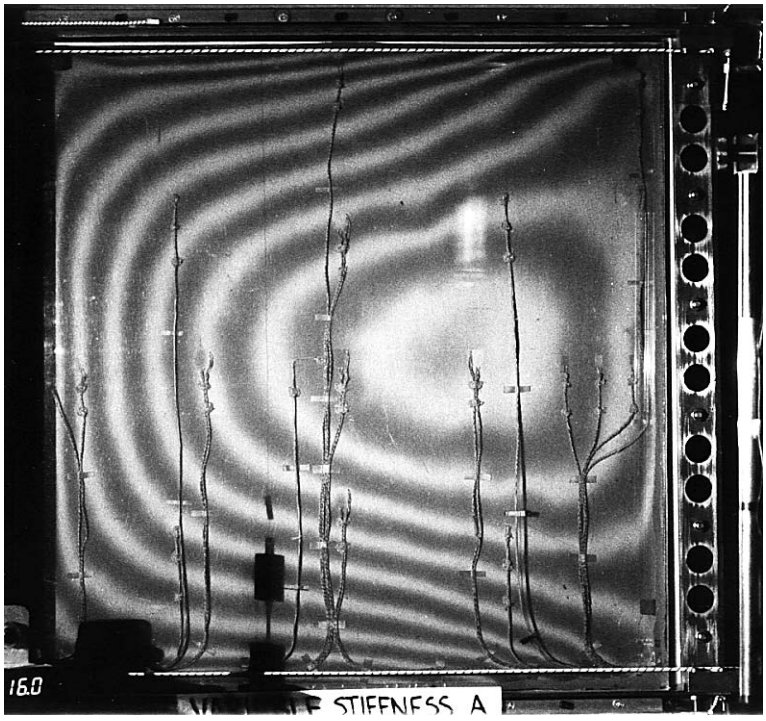


12. Shadow moiré photograph of panel with overlaps near buckling.

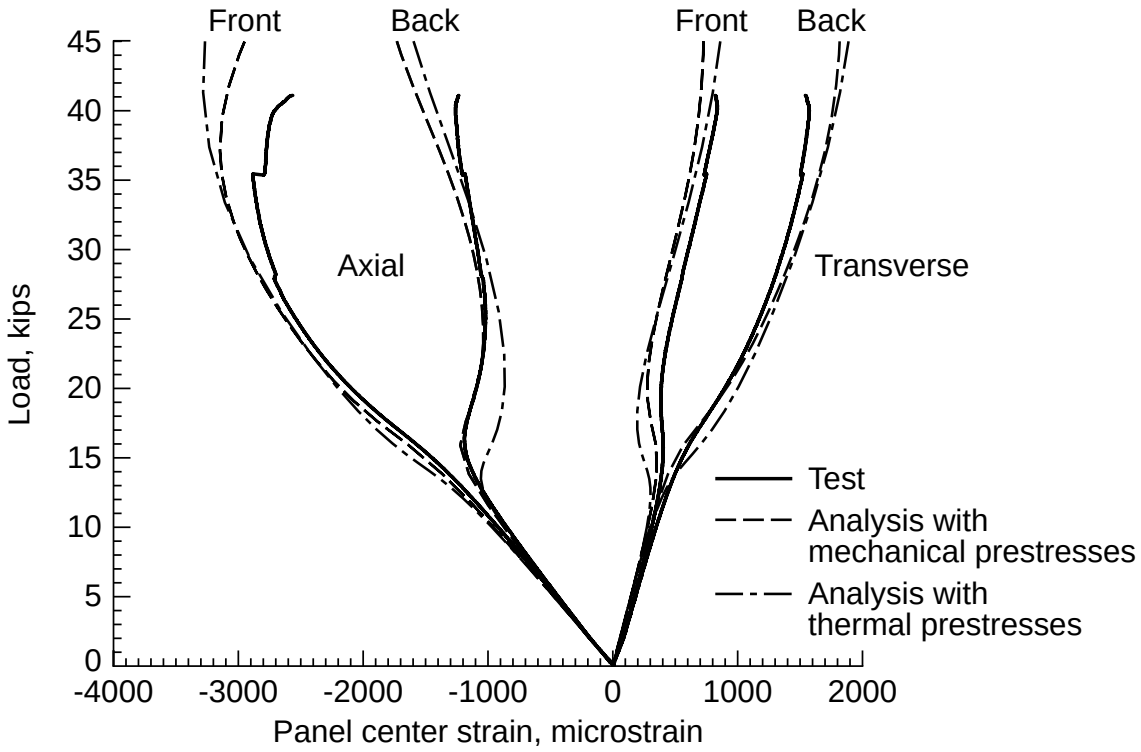


13. Panel center strain curves for panel with overlaps.

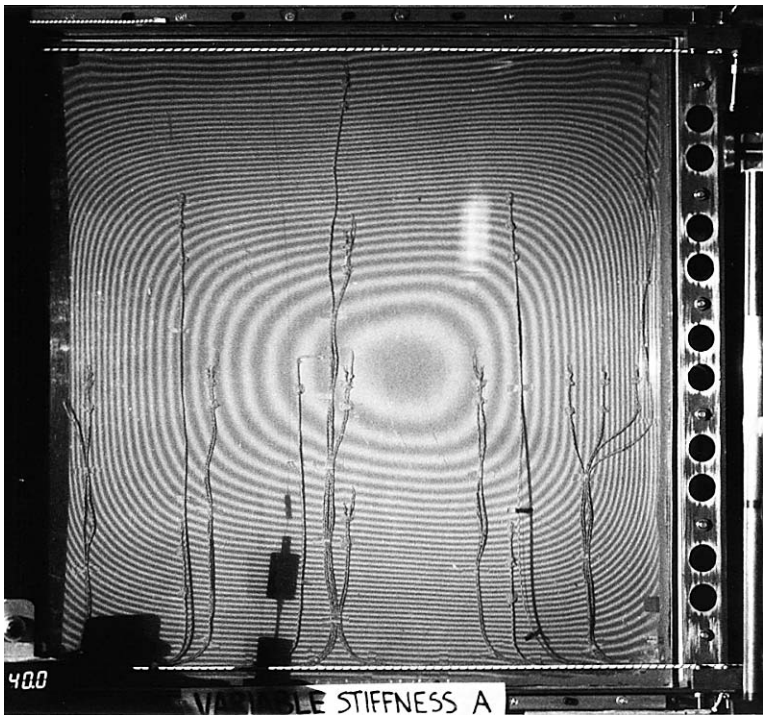


14. Shadow moiré photograph of panel with overlaps near failure.

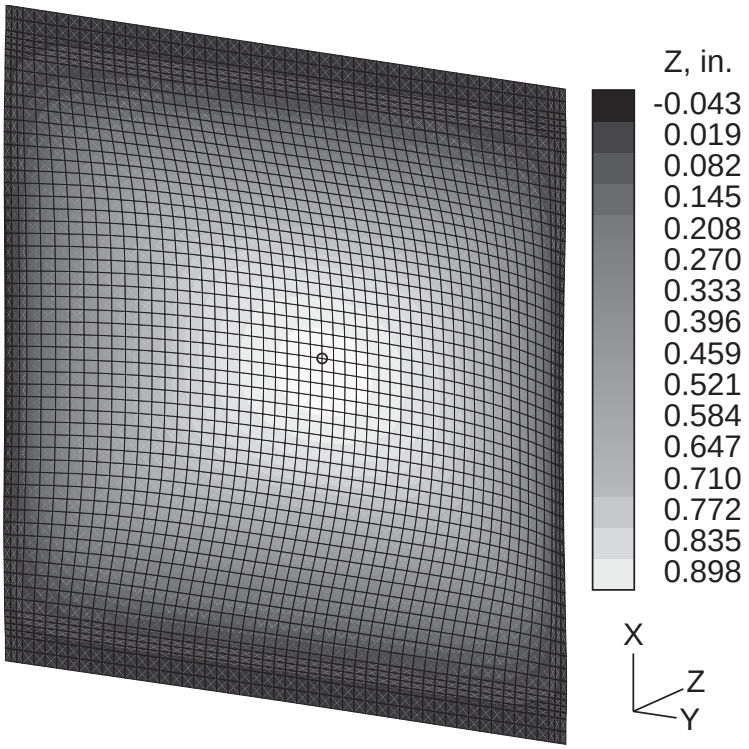


15. Predicted deflection contours for panel with overlaps.

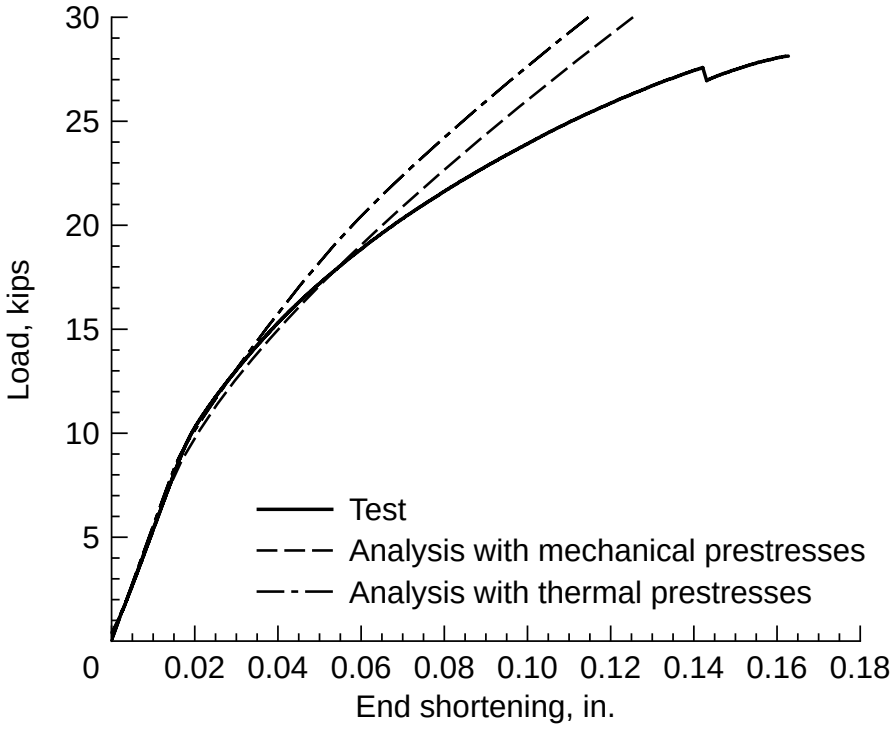


16. End shortening curves for panel without overlaps.

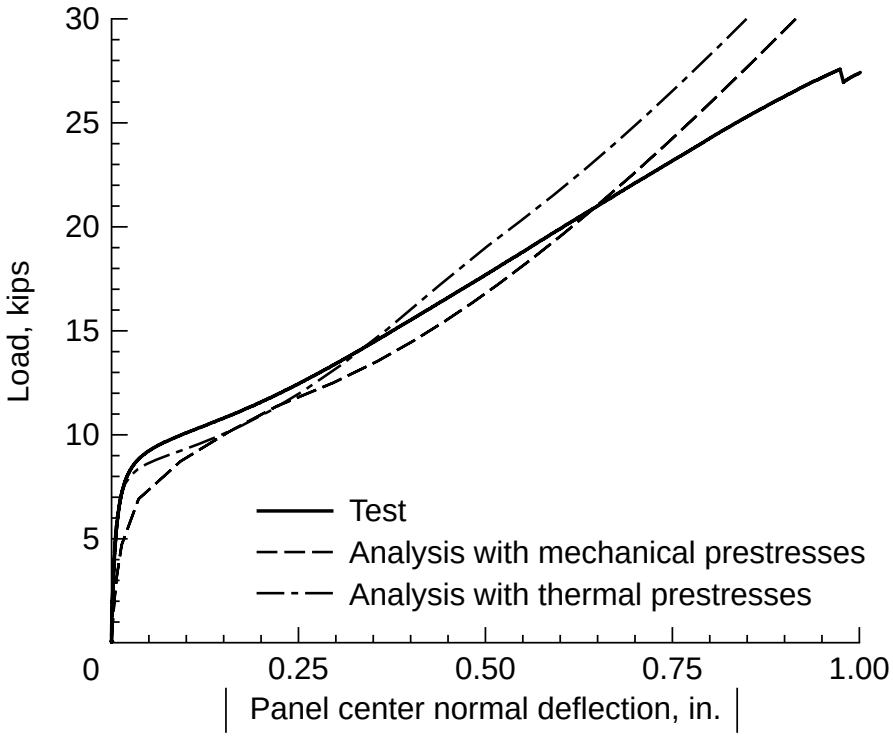


17. Panel center normal deflection curves for panel without overlaps.

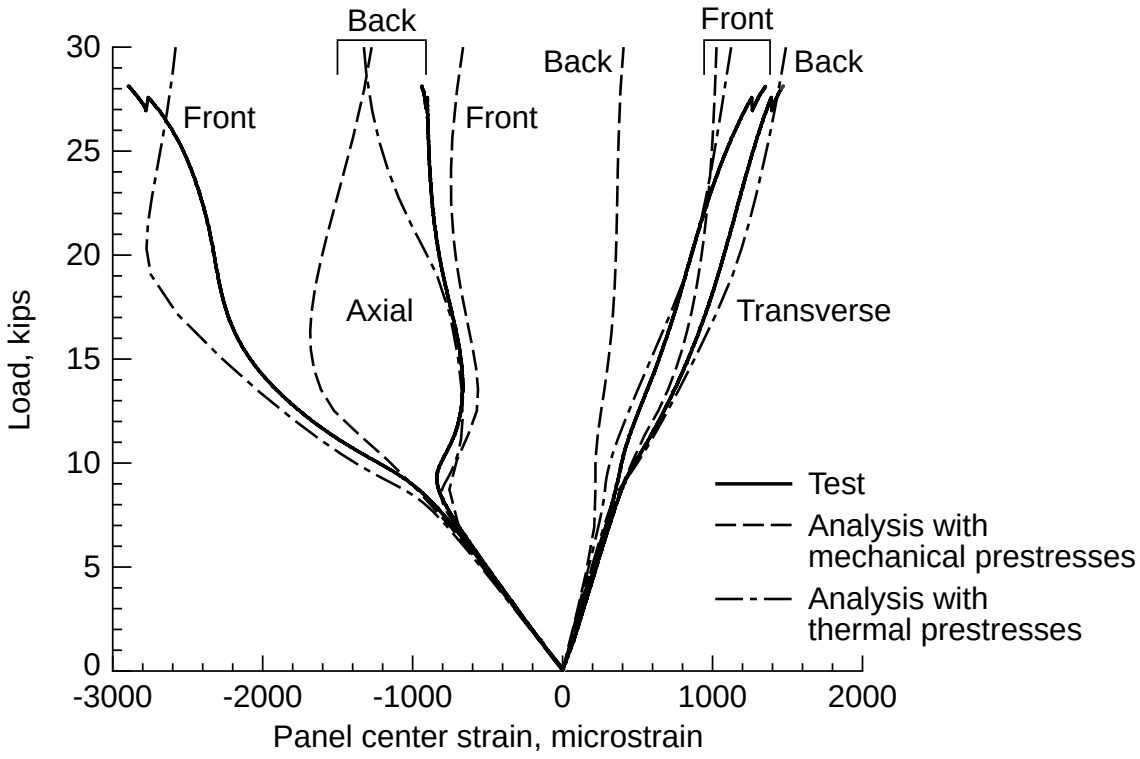


18. Panel center strain curves for panel without overlaps.